Available online at www.sciencedirect.com
SCIENCE DIRECT®
Analytical Biochemistry 341 (2005) 344–351
ANALYTICAL BIOCHEMISTRY
www.elsevier.com/locate/yabio

Noninvasive and continuous recordings of auxin fluxes in intact root apex with a carbon nanotube-modified and self-referencing microelectrode

Stefano Mancuso [a,*], Anna Maria Marras [b], Volker Magnus [c], František Baluška [d]

[a] *Dipartimento di Ortoflorofrutticoltura, Polo Scientifico, Università di Firenze, viale delle idee 30, 50019 Sesto Fiorentino (FI), Italy*
[b] *Dipartimento di Scienze Farmaceutiche, Polo Scientifico, Università di Firenze, via Ugo Schiff 6, 50019 Sesto Fiorentino (FI), Italy*
[c] *Rudier Bošković Institute, Bijenička c. 54, P.O. Box 180, HR-10002 Zagreb, Croatia*
[d] *Institute of Botany, Department of Plant Cell Biology, Rheinische Friedrich-Wilhelms University of Bonn, Kirschallee 1, D-53115 Bonn, Germany*

Received 25 January 2005
Available online 22 April 2005

Abstract

Auxin (also known as indole-3-acetic acid, IAA) represents an ancient signaling molecule of plants that also exerts bioactive actions on yeast and animal cells. Importantly, IAA emerges as a new anticancer agent due to the ability of oxidatively activated IAA to selectively kill tumor cells. IAA acts as a pheromone-like molecule in brown algae, whereas the hormone concept of IAA dominates current plant biology. However, recent advances also favor the morphogen- and transmitter-like nature of IAA in plants, making this small molecule one of the most unique molecules in the eukaryotic superkingdom. Here, we introduce new technology for the continuous measuring of IAA fluxes in living cells, tissues, and whole organs that is based on a carbon nanotube-modified and self-referencing microelectrode specific for IAA. This technique not only will advance our knowledge of how IAA regulates plant development but will also be applicable in medicine for its potential use in cancer therapy.

Keywords: Auxin; Carbon nanotube; IAA microsensor; Maize root apex; Transition zone

The plant bioregulatory molecule auxin (also known as indole-3-acetic acid, IAA)[1] plays critical roles in a variety of processes related to plant growth and development as well as in numerous physiological processes. IAA is currently considered to be a vital molecule involved in diverse processes, and researchers studying IAA need to measure dynamic IAA concentrations locally, directly, and continuously. However, the detection and determination of IAA in plant tissue are notoriously difficult due to the presence of IAA in only minute amounts; the inherent tendency of IAA to be decomposed by heat, light, and oxygen; and the presence of a wide variety of molecules that modify IAA biochemically. Because the traditional methods commonly used to measure IAA levels, such as GC [1–3], enzyme-linked immunosorbent assay (ELISA), and radioimmunoassay (RIA) [4], either are discontinuous or have other drawbacks, it is impossible to determine local in vivo concentrations of IAA in real time.

To monitor continuously the local concentrations of IAA in living plant tissues, electrochemical methods have significant advantages over the other techniques. Indeed, miniature and microelectrochemical sensors can

* Corresponding author. Fax: +39 055 4574017.
E-mail address: stefano.mancuso@unifi.it (S. Mancuso).

[1] *Abbreviations used:* IAA, indole-3-acetic acid; ELISA, enzyme-linked immunosorbent assay; RIA, radioimmunoassay; CNT, carbon nanotube; SWNT, single-walled carbon nanotube; MWNT, multi-walled carbon nanotube; DMF, *N*,*N*-dimethyl formamide; MPS, (3-mercaptopropyl)trimethoxysilane; DMSO, dimethyl sulfoxide; TIBA, 2,3,5-triiodobenzoic acid; NPA, *N*-1-naphthyphthalamic acid; BFA, brefeldin A.

0003-2697/$ - see front matter © 2005 Elsevier Inc. All rights reserved.
doi:10.1016/j.ab.2005.03.054

be positioned in proximity to the organs and cells, providing a means to estimate the local concentration of IAA. Electrochemical sensors for use in this and other applications must exhibit very high selectivity for IAA, good sensitivity, fast response times, and calibration stability and also must have a small enough size to enable placement in proximity to the studied region.

When assessing a concentration profile of IAA at different distances from the tissues, as in the case of self-referencing measurements, it is essential that the sensing tip of the device have a planar configuration so that the IAA levels at precise distances from the tissues can be determined with good spatial resolution.

The electrochemical behavior of IAA at the carbon paste and glassy carbon electrode has been reported previously [5]. Nevertheless, the responses were not satisfactory due to rather slow inhomogeneous electron transfer to the electrode. Since the discovery of carbon nanotubes (CNTs) by Iijima [6], intensive research has been conducted and has revealed several unique properties of these materials [7–11]. CNTs are molecular scale wires with high electrical conductivity, high chemical stability, and extremely high mechanical strength [12]. In general, there are two distinct types of CNTs: single-walled carbon nanotubes (SWNTs) and multiwalled carbon nanotubes (MWNTs). Use of these promising properties has led to the application of CNTs as scanning probes [13], electron field emission sources [14], nanoelectronic devices [15], batteries [16], nanotube-reinforced materials [17], and potential hydrogen storage materials [18,19]. Among this plethora of diversified applications, there has been growing interest to use CNTs as chemical sensors [20,21] owing to the ability of CNTs to promote electron transfer reactions when used as electrode material.

In this study, we used a metal (platinum) microelectrode as a substrate electrode immobilizing CNTs using (3-mercaptopropyl)trimethoxysilane (MPS) [22]. MWNT-modified electrodes have recently been shown to be suitable for highly sensitive detection of IAA in pulverized samples of plant leaves [23]. In the following sections, we demonstrate that the MWNT film shows remarkable enhancement effects on the oxidation peak current of IAA compared with a bare platinum electrode. Based on this, a highly sensitive and fast method was developed for the noninvasive and continuous monitoring of IAA fluxes in growing roots.

Material and methods

Preparation of the platinum microsensor and of the CNT-modified electrode

The procedure for the fabrication of the platinum microsensor has been reported previously [24]. A platinum wire, 10 mm long and 0.2 mm in diameter, was soldered to a silver connecting wire of the same diameter. This assembly was then mounted in a glass capillary (2 mm o.d., 1.12 mm i.d., World Precision Instruments, Sarasota, FL, USA) such that approximately 3 mm of the platinum wire protruded from the capillary tip. The microwire was secured in position by melting the glass tip of the capillary around the wire. Etching of the protruding wire to form a sharp tip was accomplished galvanically by submerging the wire for 5 s in a mixture composed of KNO_3 and 5% $KHCO_3$ melted at 600 °C. A current flow of 1.3 Å was applied between the microwire and a platinum laminar anode of approximately 1 cm^2. With a little practice with this system, we easily obtained tips with diameters of approximately 7–10 μm. Microwire insulation was achieved using an anodic electrodeposition paint (Glassophor ZQ 84-3225, BASF, Stuttgart, Germany). The probe was completed with a platinum wire, 10 mm long and 0.5 mm in diameter, acting as an auxiliary electrode and with a reference half-cell Ag/AgCl/KNO_3 (0.1 M) and NaCl (0.08 M). The cell was arranged in a three-electrode polarographic configuration that maintained the working microelectrode at a polarizing voltage of 0.7 V, ensuring a condition of diffusion-limiting current for IAA oxidation. MWNTs were purified by refluxing them in a 2-M nitric acid solution for 10 h and then were washed in twice distilled water and dried at room temperature. The MWNT suspension was prepared by dispersing the MWNTs in 2 ml of *N*,*N*-dimethyl formamide (DMF). The solution was then sonicated for 30 min to aid in the dissolution. Following Zeng and Huang [22], the bare platinum electrode was immersed in a 0.03-M (3-mercaptopropyl)trimethoxysilane (MPS) solution for 6 h and then was taken out and washed carefully with twice distilled water to remove physically adsorbed MPS. The modified electrode was prepared by dropping 5 μl of MWNT suspension on the surface of the MPS/platinum microelectrode and was left to dry.

Vibrating microelectrode system

The electrodes were turned by an angle of 45°, allowing undisturbed positive gravitropism of the root. The seedling itself remained intact. The electrical setup has been described previously [25].

Microelectrodes were set near the surface of the root at different distances from the apex, and a differential signal was calculated from data obtained while oscillating the electrode as a square wave at 0.1 Hz between two points, 10 μm apart, such that the extremes of the vibration were typically between 2 and 12 μm from the tissue surface. The electrode tip and the root apex were monitored under a microscope throughout the experiments.

Measurements of the difference in electrode voltage at the two extremes of vibration were achieved by digitizing

the electrode signals and computing the potential difference. Data were collected at a rate of 1000 data points/s.

For each electrode position, the first 2 s after the movement began was automatically discarded to eliminate stirring effects and movement artifacts, and the remaining signal was then averaged to allow the reestablishment of the gradient. The computer calculated the difference between this average and the previous one at the other extreme position and finally calculated a moving average of these differences over any desired time period.

Experiments were performed at 25 ± 0.25 °C. To prevent possible artifacts coming from temperature fluctuations, we recorded temperature changes inside the measuring chamber during all of the experiments.

Ion gradient sources for efficiency determination

An IAA source, which was used to generate a standing IAA gradient to test the efficiency of the vibrating IAA-selective microelectrode system, was constructed by filling a blunt-tipped microelectrode (tip diameter ~ 15 μm) with a solution of 50 μM IAA in 0.3%(w/v) agarose. The agarose was included in the filling medium to minimize bulk water movement into the source. This source was placed in a Petri dish and was allowed to equilibrate overnight before an IAA microelectrode was positioned perpendicular to the tip of the source pipette, and static measurements of IAA concentration were made at known points through the IAA gradient until a constant background signal was obtained. Then the electrode was repositioned to each static measurement position, and a differential signal was calculated oscillating the electrode as a square wave at 0.1 Hz between two points 10 μm apart. The static IAA within the diffusion field were modeled according to the following formula [26]:

$$C_x = C_b + \frac{(C_s - C_b)R}{R + x},$$

where C_x is the IAA concentration at a given position, C_b is the background IAA concentration in the dish, C_s is the IAA concentration at the source, R is the source radius, and x is the distance from the source. This model was compared with the statically measured values.

Calibration of the sensor and measurement of IAA fluxes and contents

The calibration of the microelectrodes was carried out in IAA solutions made by serial dilution from IAA solution. After the electrode current had reached a steady-state value, the calibration run was started in the solution with the lowest IAA concentration and proceeded toward higher activity. When the electrodes were transferred from one solution to the next one, they were blotted dry. Currents were allowed to stabilize within 10 fA before readings were taken; at the lower concentrations, stabilization took up to 1–2 s. No differences were noted among the microelectrodes prepared and tested with respect to the slope of the response or to the response time.

IAA fluxes were calculated using Fick's first law of diffusion:

$$J = \frac{D(C_1 - C_2)}{\Delta x},$$

where J is the flux rate (mol cm^{-2} s^{-1}), D is the diffusion coefficient for IAA (0.677×10^{-5} cm^2 s^{-1} at 25 °C), C_1 and C_2 are the concentrations at the two measurement positions, and Δx is the distance of measurement (cm).

Experiments were performed at 25 ± 0.25 °C. Vibrating microelectrodes were set perpendicularly to the sample (root surface), and a differential signal was calculated from data obtained while oscillating the electrodes at 0.1 Hz between two points, 10 μm apart, such that the extremes of the vibration were usually between 2 and 12 μm from the root surface.

Free IAA extraction, purification, and measurement using HPLC were conducted as described previously [27].

Plant material and inhibitor treatments

Caryopses of maize (*Zea mays* L. cv. Gritz, Maïsadour semences, France) were soaked overnight in aerated tap water and placed between damp paper towels in Petri dishes. Dishes were maintained in a vertical position, incubated at 26 °C for 48 h, and used after seedling roots reached a length of approximately 5–7 cm. For pharmacological experiments, root apices were submerged in appropriate solutions at room temperature. The amount of dimethyl sulfoxide (DMSO) used to dissolve IAA and IAA transport inhibitors was maintained at 0.1%(v/v) of the final concentration.

Results

Electrochemical behavior of microelectrodes

The microelectrodes fabricated were initially tested in distilled water. Fig. 1 shows a polarogram graph obtained by a comparison of the current with the voltage. When the IAA microelectrode was polarized in a concentration of 5 μM IAA in pure water and with a voltage sweep from 0 to 1 V, it showed an oxidation peak in the range of 0.65–0.75 V with an output of approximately 40 pA (depending on the tip radius). During subsequent experiments, the microelectrode was polarized at a voltage of 700 mV, ensuring the condition of diffusion-limiting current for dissolved IAA oxidization, with the latter being linearly dependent on IAA concentration.

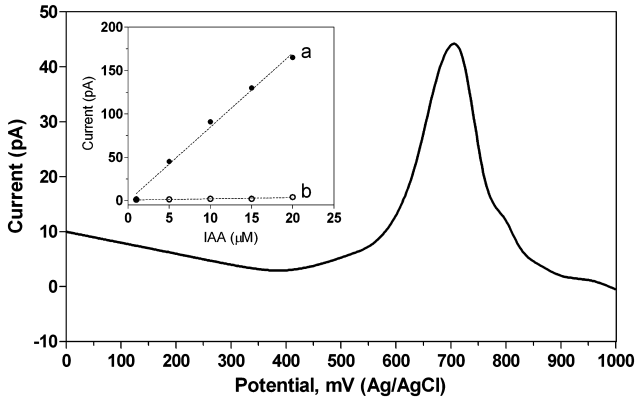

Fig. 1. Representative polarogram for the oxidation of IAA, showing the response of the MWNT-modified microelectrode current to the applied potentials. The polarogram was obtained by placing the electrode in a solution containing 5×10^{-6} M IAA. The inset shows a representative calibration plot of a microelectrode in the range of 1–20 μM.

The electrocatalytic ability of MWNTs makes possible the amperometric measurements of IAA. In the Fig. 1 inset, the amperometric responses of the MWNT-modified microelectrode (trace a) and the bare MPS–platinum electrode (trace b) are compared in the IAA concentration range of 1–20 μM. As expected from preliminary experiments (data not shown), the bare platinum electrode is not responsive to the changes in IAA concentration. In contrast, the MWNT electrode responds rapidly to changes in IAA concentration and shows a linear dependence ($r^2 = 0.9932$) in the IAA concentration range of 1–20 μM. The detection limit of the electrode is 0.1 μM, with a signal-to-noise level of 3.

Influence of amount of MWNTs

The MWNTs cast film thickness is determined by the amount of MWNT–DMS dispersion on the MPS–platinum surface. By increasing the amount of the MWNT–DMS dispersion (representing the content of MWNT on the electrode surface), it is possible to also increase the number of catalytical sites for the IAA oxidation. Fig. 2A shows that the amount of MWNTs used has an influence on the peak current. The oxidation peak was

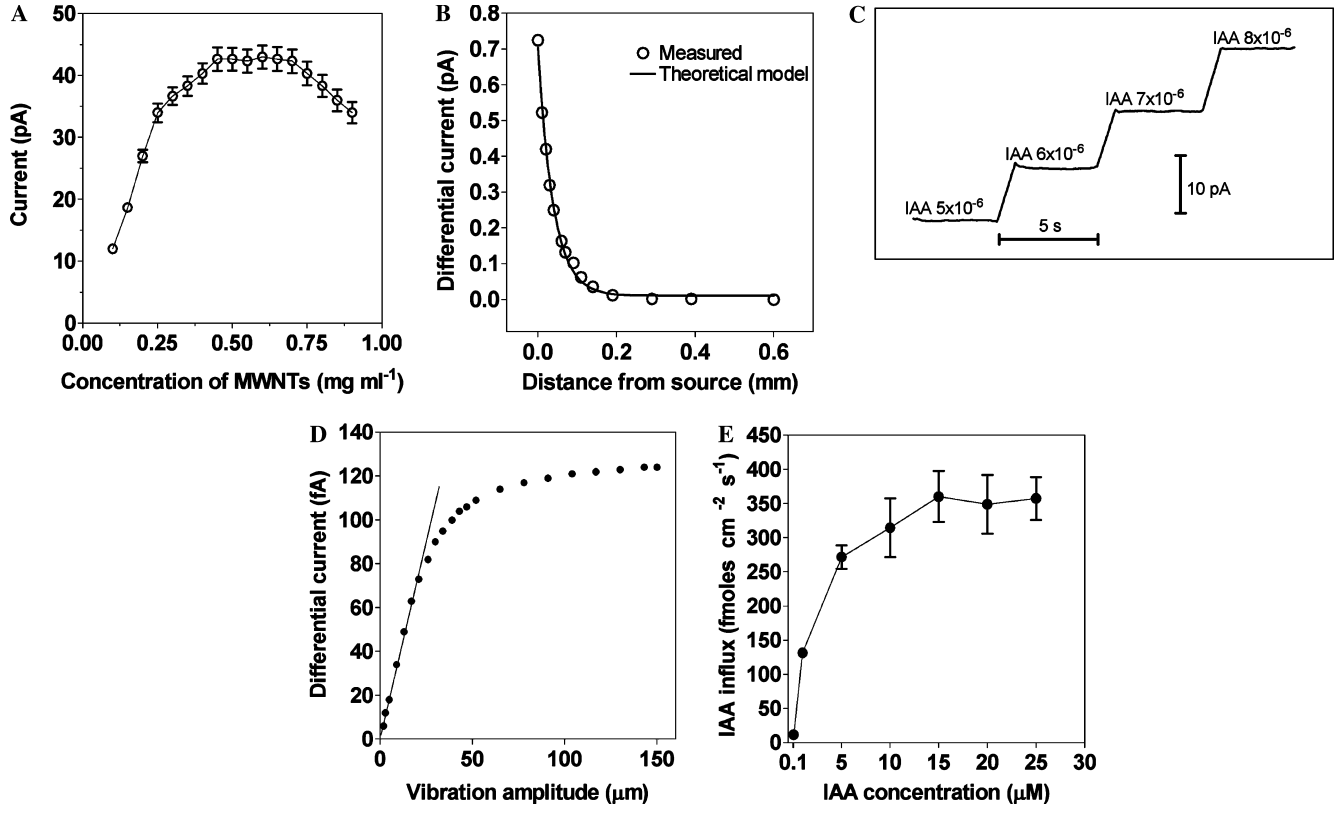

Fig. 2. (A) Influence of the MWNT concentration (mg ml^{-1}) used on the anodic peak current. Other conditions are the same as in Fig. 1. Data shown are means of 10 replicates. Error bars represent standard errors. (B) Theoretical and experimental measurements of an IAA gradient as a function of distance from an artificial IAA gradient source. (C) Response time for the MWNT-modified microelectrode to the successive increment of 1 μM of IAA. Operating potential is 0.7 V. (D) Local IAA concentration as a function of the distance from a root cell. Data were collected by changing the microelectrode vibration amplitude between 0 and 150 μm at 0.1 Hz, 1.5 mm from the root cap junction in 5×10^{-6} M IAA. (E) Saturation of IAA transport measured as a function of the IAA influx in the transition zone of root apex, with increasing amounts of IAA in the external solution. Differential current from an IAA-selective microelectrode placed 2 μm from the root surface and used in a self-referencing mode is shown. The sensor was vibrated between two positions 10 μm apart at a rate of 0.1 Hz. Positive differential currents mean a net IAA influx. Data shown are means of 10 replicates. Error bars represent standard errors.

reasonably high even when we used 0.3 mg ml^{-1} of MWNT–DMS dispersion to cast the GCE. On further increasing the amount of MWNT–DMS dispersion, the peak current increased further and remained nearly stable after reaching 0.4 mg ml^{-1}. However, the cast film becomes thicker and blocks the electron transfer when the amount of MWNT–DMS dispersion exceeds 0.7 mg ml^{-1}.

Selectivity

The selectivity of the microelectrode toward numerous interferents was verified with the concentration of IAA maintained at 5×10^{-6} M. A solution containing the interferent at a fixed concentration of 10^{-3} M was used. The results of different interferents are summarized in Table 1. Many compounds usually contained in nutritive solutions do not interfere with the IAA microelectrode (signal change < 4%). Therefore, the selectivity shown makes the electrode functional for practical applications.

Artificial source of IAA fluxes and efficiency measurement

A micro-IAA source was used to generate an IAA gradient in solution, and then a series of static readings were taken at different known distances from the gradient source to characterize the gradient. Subsequently, the same gradient was measured oscillating the same electrode (Fig. 2B). This approach determines the efficiency of the self-referencing IAA microelectrode for detecting a specific IAA gradient. Comparisons of measured fluxes with those determined from the static measurements typically showed, for the self-referencing electrode, an underestimation of the IAA fluxes ranging from 5 to 23%. These values were typical for each electrode and were taken into account in all calculations.

Table 1
Effect of interferents on the relative current intensity of MWNT-modified microelectrodes

Interferent[a]	Relative current change value (%, $[C_2 - C_1]/C_2 \times 100$)[b]
$Ca(NO_3)_2$	1.33 ± 0.13
NaH_2PO_4	2.11 ± 0.31
$MgSO_4$	2.01 ± 0.16
KCl	0.34 ± 0.05
$CuSO_4$	−0.47 ± 0.05
KH_2PO_4	−1.34 ± 0.16
KNO_3	0.21 ± 0.03
$MnCl_2$	0.55 ± 0.02
NaN_3	2.23 ± 0.36
Sucrose	2.52 ± 0.21
Glucose	4.03 ± 0.49
NPA	3.56 ± 0.23
BFA	2.35 ± 0.32
TIBA	4.23 ± 0.37
NAA	−5.32 ± 0.55
2,4-D	−3.69 ± 0.31

Note. Values are means and standard deviations ($n = 5$).
[a] Each solution contains a fixed IAA concentration of 5×10^{-6} M and an interferent concentration of 10^{-3} M except for $Ca(NO_3)_2$ (10^{-2} M) and KCl (10^{-2} M).
[b] C_2 and C_1 are the current intensities using the 5×10^{-6} M IAA solutions without and with interferents, respectively.

Response time

After the microsensor had reached a steady current in 50 ml of well-stirred 5×10^{-6} M IAA solution, a small aliquot of IAA was added to the solution, producing a small step of IAA concentration increase. The electrode current change followed. A typical trace of the current changes following the addition of exogenous IAA is shown in Fig. 2C.

Determination of IAA in plant roots

To test the practical application of the IAA sensor, it was used to quantify IAA in root samples of different species. The measurements were also carried out for control with HPLC. The results in Table 2 show that the determinations of IAA by HPLC and by IAA sensor are very close.

Measurements of local IAA concentration

Because the procedure for the flux measurement is based on the assumption that both of the extreme positions of the electrode tip during the "self-referencing movement" are inside the diffusion layer, IAA concentration was measured as a function of the distance from the root surface. For this purpose, the electrode vibration amplitude was increased in steps of 10 μm. The electrode was first positioned in direct contact with the cell wall of an epidermis single cell (average diameter> 50 μm) located at the root surface. Then the electrode was moved back 2 μm, and this was the zero starting point of the vibration. The amplitude of the first set of oscillations was 10 μm beginning from the zero starting point, and the amplitudes of subsequent ones were increased in steps of 10 μm. The maximum amplitude reached was 150 μm. The results plotted in Fig. 2D show that with the oscillation amplitude selected for the flux measurements (2–12 μm) throughout this work, the

Table 2
Determination of IAA in root samples by HPLC and the IAA sensor

Root sample	IAA by HPLC[a] (ng/g)	IAA by sensor (ng/g)
Maize	46.3 ± 3.3	52.5 ± 4.3
Arabidopsis	65.4 ± 5.4	59.8 ± 3.9
Walnut	86.2 ± 7.3	89.8 ± 7.9

Note. Values are means and standard deviations ($n = 5$).
[a] Free IAA measured as described in [27].

upper position of the electrode is inside the diffusion layer. Therefore, Fick's first law can be applied to calculate the flux.

Transport saturation

Net IAA influxes measured in the transition zone of the roots over a range of increasing concentrations (1–25 μM) of IAA yielded concentration-dependent kinetics (Fig. 2E). The influx of external IAA was saturated at a concentration of 15 μM, suggesting that IAA transport to the root tissue is carrier mediated. A similar saturation of IAA uptake into maize root apices also was scored using radioactive IAA when the saturable uptake was greatest in the root segment corresponding to the transition zone (2–4 mm), whereas the nonsaturable uptake was similar throughout the entire root growth zone (2–10 mm) [28].

IAA fluxes in intact root apices

The sensitivity of the vibrating IAA-selective microelectrode based on CNTs was examined further by measuring IAA fluxes at different positions along an intact root. In spite of some differences in the quantitative characteristics, all root apices showed the same spatial organization in net IAA influxes. The IAA flux profile along the root apex is shown in Fig. 3. Typically, IAA influxes showed a distinct peak at 1.0–1.5 mm from the root apex. This root region is called the transition zone due to the cessation of cell divisions and the preparation of cells for rapid cell elongation [29–31]. This transition zone peak averaged 372 ± 48 fmol cm^{-2} s^{-1} ($n = 10$), whereas at the more distal positions corresponding to cells accomplishing their onset into rapid cell elongation (>2.5 mm), the IAA influx was smaller at 28 ± 14 fmol cm^{-2} s^{-1} ($n = 10$) and remained the same at positions as far back as 5 mm from the root apex.

To further probe the IAA microelectrode, we took advantage of some well-characterized auxin transport inhibitors [32–34], such as 2,3,5-triiodobenzoic acid (TIBA) and *N*-1-naphthyphthalamic acid (NPA), as well as of the inhibitor brefeldin A (BFA), which blocks exocytic delivery of vesicles to the plasma membrane and inhibits IAA transport from cell to cell. Inhibition of IAA transport due to the exposure of the root apex to both TIBA (100 μM) and BFA (100 μM) considerably inhibited IAA influxes into cells of the transition zone of maize root apices. The influxes measured in the transition zone of the root apex after 2 h of treatment were approximately 57 ± 14 fmol cm^{-2} s^{-1} (TIBA, $n = 10$) and 86 ± 9 fmol cm^{-2} s^{-1} (BFA, $n = 10$) and were significantly different ($P < 0.001$) from the influxes recorded in control root apices (372 ± 48 fmol cm^{-2} s^{-1}). NPA treatment (50 μM) inhibited IAA influxes in the transition zone, but to a less significant extent, with the control influx decreasing to 220 ± 23 fmol cm^{-2} s^{-1} ($n = 10$) (Fig. 3).

Importantly, in addition to the punctual flux measurements, the self-referencing IAA microelectrodes can be used to obtain "topographical" images of the IAA

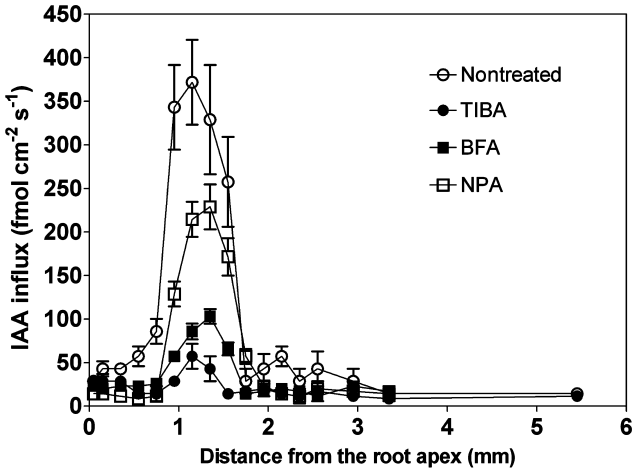

Fig. 3. Diagram illustrating the IAA influx profile along a single root and the effects of TIBA (100 μM for 2 h), BFA (100 μM for 2 h), and NPA (50 μM for 2 h) in a condition of IAA saturation transport (external concentration 15 μM IAA). Differential current from an IAA-selective microelectrode placed 2 μm from the root surface and used in a self-referencing mode is shown. The sensor was vibrated between two positions 10 μm apart at a rate of 0.1 Hz. Positive differential currents represent a net IAA influx. Data shown were collected continuously over a 10-min period and are means of 10 replicates. Error bars represent standard errors. In all cases where error bars do not overlap, Student's *t* tests show samples to be significantly different at $P < 0.05$ or better.

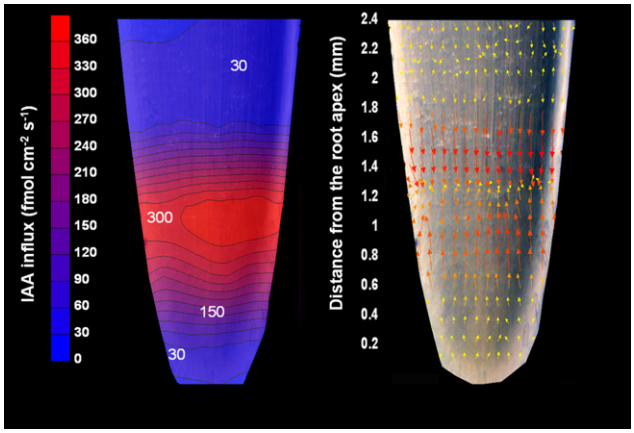

Fig. 4. Contour map (left) and vector map (right) showing IAA influxes into the root apex of maize. The data were recorded oscillating the electrode as a square wave at 0.1 Hz between two points 10 μm apart. The electrode was moved in the *x* direction collecting data every 100 μm. After finishing one pass, the microelectrode was moved 50 μm in the *y* direction and then returned in the opposite *x* direction. Both maps were constructed using the position data of the microsensor that were recorded by the data acquisition system together with the current output. Scattered x, y, z data were interpolated by using Surfer software (Golden Software, Golden, CO, USA).

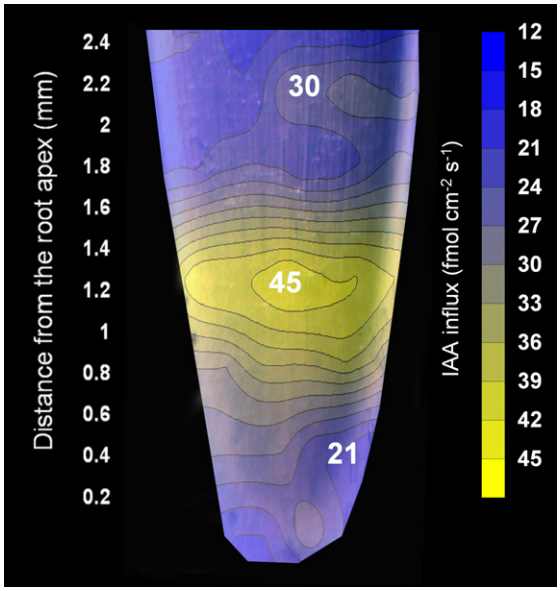

Fig. 5. Contour map showing the effect of TIBA (100 μM for 2 h) on the IAA influxes into the root apex of maize. Conditions were identical to those in Fig. 4.

influxes into the root apex. Using the microelectrode position data that were collected along with the electrode output by the data acquisition system, a high-resolution contour plot of IAA influxes can be obtained (Fig. 4). From the contour map, the localization of a peak in the IAA influx localized in the transition zone of the root apex is obvious. The ability of TIBA to block IAA influx was also tested, and a concentration of 100 μM was found to drastically reduce the influxes of IAA into the transition zone as compared with the untreated controls (Fig. 5).

Discussion

In the current work, we have provided results that demonstrate the effectiveness of an IAA-selective self-referencing microelectrode as a research tool to study IAA transport in biological systems. The CNT-modified electrode described in this article is inexpensive, is easy to prepare, and demonstrates high sensitivity in detecting IAA. Despite the fact that the technique did not show higher sensitivity than HPLC, the use of an IAA-selective microelectrode will allow one to monitor continuously in vivo and noninvasively the local concentrations of IAA in living plant tissues. To make reliable measurements with IAA microsensors, a number of controls are necessary. Great care was taken in developing a sensor that not only can perform on a time scale compatible with the self-referencing technique but also has sufficient selectivity for IAA in specific experimental conditions. Moreover, the microelectrode was used in a root region where there is evidence of the presence of IAA fluxes, and the electrochemical signal was consistent with this species. Finally, the signal was characterized by appropriate pharmacological experiments.

Currently, our understanding of IAA is expanding dramatically, and the classical hormonal status of IAA is moving toward also viewing this powerful bioregulatory molecule as an ancient signaling molecule [35], a morphogen [36], and even a neurotransmitter-like substance [31,37,38]. Besides regulating gene expression via specific transcription factors, short-lived regulatory shuttling proteins, and IAA-responsive promoters [39], IAA is well known to be transported from cell to cell in a complex process based on vesicular trafficking [37–40]. In this respect, it is important that IAA applied on plant cells from the outside elicits rapid electrical signals and calcium transients via controlling activities of ion channels [41]. All of this, combined with the recent discoveries linking polar transport of IAA tightly with vesicular trafficking, strongly suggests that IAA may act as a transmitter of cell-to-cell communication in plants [40].

To understand all of the diverse roles played by IAA, we must quantify both local amounts and fluxes of IAA in intact organs. The most fascinating property of IAA is its polar cell-to-cell transport, first requiring its efflux from one cell and then requiring subsequent influx into the adjacent cell [31,37]. It is becoming very clear that this polar transport of IAA is essential for growth and morphogenesis of plant cells and organs as well as of the whole plant body [42,43]. CNT-modified and self-referencing microelectrodes allow noninvasive recordings of IAA fluxes at the intact root apex, revealing that cells differ dramatically in their abilities to transport IAA. In the root apex, the most dramatic IAA influx was recorded at a distance of approximately 1–2 mm from the root cap junction. These unique root cells terminate their mitotic activity and traverse the so-called transition zone, which is critical for several sensory properties of root apices (e.g., monitoring of gravity and light) [29,32].

In conclusion, the ability to perform noninvasive in vivo recordings of IAA fluxes over intact plant root apices provides us with a critical tool for deepening our understanding of how IAA drives the growth of plant organs.

Acknowledgments

Financial support to AGRAVIS by the Deutsche Agentur für Raumfahrtangelegenheiten (DARA, Bonn, Germany) and the Ministerium für Wissenschaft und Forschung (MWF, Düsseldorf, Germany) is gratefully acknowledged. František Baluška receives partial support from the Slovak Academy of Sciences (grant agency VEGA, grant 2031, Bratislava, Slovakia).

Appendix A. Supplementary data

Supplementary data associated with this article can be found, in the online version, at doi:10.1016/j.ab.2005.03.054.

References

[1] W.J. Hunter, High-performance gas chromatographic method for the estimation of the indole-3-acetic acid content of plant materials, J. Chromatogr. A 362 (1986) 430–435.

[2] P. Hedden, Modern methods for the quantitative analysis of plant hormones, Annu. Rev. Plant Physiol. 44 (1993) 107–129.

[3] F.G. Sanchez, A.N. Diaz, A.J. Pareja, Micellar liquid chromatography of plant growth regulators detected by derivative fluorometry, J. Chromatogr. A 723 (1996) 227–233.

[4] E.W. Weiler, Immunoassay of plant growth regulators, Annu. Rev. Plant Physiol. 35 (1984) 85–95.

[5] F. Hernandez, F. Galan, L. Nieto, L. Hernandez, Direct determination of indole-3-acetic acid in plant tissues by electrochemical techniques using a carbon-paste modified with OV-17 electrode, Electroanalysis 6 (1994) 577–583.

[6] S. Iijima, Helical microtubules of graphitic carbon, Nature 354 (1991) 56–58.

[7] N.G. Chopra, L.X. Benedict, V.H. Crespi, M.L. Cohen, S.G. Louie, A. Zettl, Fully collapsed carbon nanotubes, Nature 377 (1995) 135–138.

[8] A. Thess, R. Lee, P. Nikolaev, H. Dai, P. Petit, J. Robert, C. Xu, Y.H. Lee, S.G. Kim, A.G. Rinzler, D.T. Colbert, G.E. Scuseria, D. Tomanek, J.E. Fischer, R.E. Smalley, Crystalline ropes of metallic carbon nanotubes, Science 273 (1996) 483–487.

[9] E.W. Wong, P.E. Sheehan, C.M. Lieber, Nanobeam mechanics: elasticity, strength, and toughness of nanorods and nanotubes, Science 277 (1997) 1971–1975.

[10] J. Liu, A.G. Rinzler, H. Dai, J.H. Hafner, R.K. Bradley, P.J. Boul, A. Lu, T. Iverson, K. Shelimov, C.B. Huffman, F. Rodriguez-Macias, Y.-S. Shon, T.R. Lee, D.T. Colbert, R.E. Smalley, Fullerene pipes, Science 280 (1998) 1253–1256.

[11] R.H. Baughman, C. Cui, A.A. Zakhidov, Z. Iqbal, J.N. Barisci, G.M. Spinks, G.G. Wallace, A. Mazzoldi, D. De Rossi, A.G. Rinzler, O. Jaschinski, S. Roth, M. Kertesz, Carbon nanotube actuators, Science 284 (1999) 1340–1344.

[12] P.M. Ajayan, Nanotubes from carbon, Chem. Rev. 99 (1999) 1787–1800.

[13] H. Dai, J.H. Hafner, A.G. Rinzler, D.T. Colbert, R.E. Smalley, Nanotubes as nanoprobes in scanning probe microscopy, Nature 384 (1996) 147–150.

[14] W.A. De Heer, A. Chatelain, D.A. Ugarte, Carbon nanotube field-emission electron source, Science 270 (1995) 1179–1180.

[15] S. Tans, A. Verschueren, C. Dekker, Room-temperature transistor based on a single carbon nanotube, Nature 393 (1998) 49–52.

[16] G.L. Che, B.B. Lakschmi, E.R. Fisher, C.R. Martin, Carbon nanotube membranes for electrochemical energy storage and production, Nature 393 (1998) 346–349.

[17] M.S. Dresselhaus, Down the straight and narrow, Nature 358 (1992) 195–198.

[18] P. Chen, X. Wu, J. Lin, K.L. Tan, High H_2 uptake by alkali-doped carbon nanotubes under ambient pressure and moderate temperatures, Science 285 (1999) 91–93.

[19] C. Liu, Y.Y. Fan, M. Liu, H.T. Cong, H.M. Cheng, M.S. Dresselhaus, Hydrogen storage in single-walled carbon nanotubes at room temperature, Science 286 (1999) 1127–1129.

[20] J. Kong, N. Franklin, C. Zhou, S. Peng, J.J. Cho, H. Dai, Nanotube molecular wires as chemical sensors, Science 287 (2000) 622–625.

[21] P.E.M. Phillips, R.M. Wightman, Critical guidelines for validation of the selectivity of in vivo chemical microsensors, Trends Anal. Chem. 22 (2003) 509–514.

[22] B. Zeng, F. Huang, Electrochemical behaviour and determination of fluphenazine at multi-walled carbon nanotubes/(3-mercaptopropyl) trimethoxysilane bilayer modified gold electrodes, Talanta 64 (2004) 380–386.

[23] K. Wu, Y. Sun, S. Hu, Development of an amperometric indole-3-acetic acid sensor based on carbon nanotubes film coated glassy carbon electrode, Sens. Actuat. B 96 (2003) 658–662.

[24] S. Mancuso, M. Boselli, Characterisation of the oxygen fluxes in the division, elongation, and mature zone of Vitis roots: influence of oxygen availability, Planta 214 (2002) 767–774.

[25] S. Mancuso, G. Papeschi, A.M. Marras, A polarographic, oxygen-selective, vibrating-microelectrode system for the spatial and temporal characterisation of transmembrane oxygen fluxes in plants, Planta 211 (2000) 384–389.

[26] S.C. Land, D.M. Porterfield, R.H. Sanger, P.J.S. Smith, The self-referencing oxygen-selective microelectrode: detection of transmembrane oxygen flux from single cells, J. Exp. Biol. 202 (1999) 211–218.

[27] K.N. Mwange, H.-W. Hou, K.-M. Cui, Relationship between endogenous indole-3-acetic acid and abscisic acid changes and bark recovery in *Eucommia ulmoides* Oliv. after girdling, J. Exp. Bot. 54 (2003) 1899–1907.

[28] H.V. Martin, P.-E. Pilet, Saturable uptake of indol-3yl-acetic acid by maize roots, Plant Physiol. 81 (1986) 889–895.

[29] F. Baluška, D. Volkmann, P.W. Barlow, Specialized zones of development in roots: view from the cellular level, Plant Physiol. 112 (1996) 3–4.

[30] F. Baluška, D. Volkmann, P.W. Barlow, A polarity crossroad in the transition growth zone of maize root apices: cytoskeletal and developmental implications, J. Plant Growth Regul. 20 (2001) 170–181.

[31] F. Baluška, P. Wojtaszek, D. Volkmann, P.W. Barlow, The architecture of polarized cell growth: the unique status of elongating plant cells, BioEssays 25 (2003) 569–576.

[32] K.S. Thomson, R. Hertel, S. Muller, J.E. Tavares, 1-Naphthylphthalamic acid and 2,3,5-triiodobenzoic acid: in vitro binding to particulate cell fractions and action on auxin transport in corn coleoptiles, Planta 109 (1973) 337–352.

[33] M.R. Sussman, M.H.M. Goldsmith, The action of specific inhibitors of auxin transport on uptake of auxin and binding of *N*-1-naphthylphthalamic acid to a membrane site in maize coleoptiles, Planta 152 (1981) 13–18.

[34] D.A. Morris, Transmembrane auxin carrier systems: dynamic regulators of polar auxin transport, Plant Growth Regul. 32 (2000) 161–172.

[35] T.J. Cooke, D.B. Poli, A.E. Sztein, J.D. Cohen, Evolutionary patterns in auxin action, Plant Mol. Biol. 49 (2002) 319–338.

[36] R.P. Bhalerao, M.J. Bennett, The case for morphogens in plants, Nat. Cell Biol. 5 (2003) 939–943.

[37] F. Baluška, J. Šamaj, D. Menzel, Polar transport of auxin: carrier-mediated flux across the plasma membrane or neurotransmitter-like secretion?, Trends Cell Biol. 13 (2003) 282–285.

[38] F. Baluška, S. Mancuso, D. Volkmann, P.W. Barlow, Root apices as plant command centres: the unique "brain-like" status of the root apex transition zone, Biologia (Bratislava) 59 (2004) 7–19.

[39] G. Hagen, T. Guilfoyle, Auxin-responsive gene expression: genes, promoters, and regulatory factors, Plant Mol. Biol. 49 (2002) 373–385.

[40] N. Geldner, N. Anders, H. Wolters, J. Keicher, W. Kornberger, P. Muller, A. Delbarre, T. Ueda, A. Nakano, G. Jurgens, The Arabidopsis GNOM ARF–GEF mediates endosomal recycling, auxin transport, and auxin-dependent plant growth, Cell 112 (2003) 219–230.

[41] D. Becker, R. Hedrich, Channelling auxin action: modulation of ion transport by indole-3-acetic acid, Plant Mol. Biol. 49 (2002) 349–356.

[42] J. Friml, Auxin transport: shaping the plant, Curr. Opin. Plant Biol. 6 (2003) 7–12.

[43] R. Swarup, M.M. Bennett, Auxin transport: the fountain of life in plants?, Dev. Cell 5 (2003) 824–826.